Effect of dopant and binder on the formation of ZnO powders during thermal decomposition of spray dried zinc acetate based granules

Ş. DUMAN*, B. ÖZKAL
[a]*Department of Metallurgical & Materials Engineering, Particulate Materials Laboratories, Istanbul Technical University, 34469 Istanbul, Turkey*

This paper investigates the effects of dopant and binder on the structural and optical properties of ZnO nanopowders synthesized from zinc acetate based solution via consecutive processes of spray drying and thermal decomposition. The ultimate powders were characterized to compare powder properties. In addition, structural and optical characterization of the powders was performed via XRD and UV-Vis spectrophotometer. The results have shown that irregular powder morphology obtained after the decomposition of sole zinc acetate, can be transformed to regular fiber morphology in presence of certain additions. Furthermore, it was demonstrated that both PVA and the dopants ($AgNO_3$ and H_3BO_3) used in this study were effective on final L/D ratios of fibers and the specific surface area values of final powders obtained.

(Received April 7, 2016; accepted August 3, 2016)

Keywords: ZnO nanofibers, Spray drying, Thermal decomposition

1. Introduction

Nanoscale zinc oxide (ZnO) is one of the interesting functional materials and widely demanded for fabrication of various applications including varistors [1-3], solar cells [1, 2], gas sensors [3-5] and optoelectronics [6]. As a multifunctional material, it has the wide band gap (3.37 eV), high exciton binding energy (60 meV), high electron feature, and shows optical transparency [2, 3, 7].

Doping and morphological features like the control of shape and size of the nanoparticles are very important for improving crystallization quality and optical, electrical and magnetic properties of ZnO [3, 8].

Besides, previous studies have indicated that Ag as a dopant behaves as a superior compensation of native defects in ZnO and enhances structural and optical properties [9, 10]. Among other dopants, boron or boron-rich compound doped ZnO can improve characteristics and the electronic properties and photocatalytic activity [11, 12]. Boron has peerless chemical and physical properties, and can behave as interstitial and substituted boron in ZnO lattice due to the smaller ion radius of boron [13]. In literature, various transition metals (TMs) or transition metal oxides (TMOs) as silver, copper and boron-rich compound have been doped ZnO-PVA to form composite [14]. Poly-vinyl alcohol (PVA) is preferred as polymer due to its water-soluble, nontoxic and degradable material.

Various methods have been employed to grow a variety of ZnO nanostructures, including nanowires, nanorods, nanoflowers and other complex morphologies [15-17]. Several methods for the synthesis of ZnO and doped with TMs or TMOs have been reported such as preparation of fine ZnO by means of spray pyrolysis [5, 18], sol-gel technique [6, 19, 20], and thermal decomposition [21]. The homogeneity and uniform distribution is vital issue to obtain well-dispersed TMs or TMOs and polymer doped ZnO particles with controlled size and shape. Selection of precursors has also affected size and shape of undoped and doped ZnO particles. ZnO particles have been synthesized from aqueous solutions of different zinc precursors; commonly zinc acetate, zinc nitrate, zinc sulfate, zinc chloride or zinc oxalates [20, 22]. Metal salts (acetate, nitrate, oxalate or sulfate, etc.) and generally PVA polymer have been used in the synthesizing TMs or TMOs and polymer doped ZnO particles.

It has been reported in literature that homogeneous granules is commonly fabricated by spray drying that is transformed from feed slurry to a dry granules by spraying into hot medium. This method has been commonly preferred due to its advantage of the rapid solvent evaporation during production [23-25].

As compared with nanocomposite materials prepared by aforementioned methods, the materials prepared by spray drying possess average particle size and narrow size distribution, high purity, and the possibility to obtain high quality granules [26]. Spray drying and consecutive thermal decomposition combination was successfully applied to prepare some electrode materials [26-28]. However, combining processes spray drying and thermal decomposition in air is a new method used in the synthesis of ZnO based nanomaterials and there are not many

studies in the literature.

The present study reports the formation of ZnO particles during thermal decomposition of spray dried zinc acetate based granules. Effect of different dopants and presence of PVA were investigated during characterization of the ultimate powders properties.

2. Experimental details

2.1 Material synthesis

Zinc acetate dehydrate ($Zn(CH_3COO)_2 \cdot 2H_2O$ Alfa Aesar^{TM}), silver nitrate ($AgNO_3$) , Alfa Aesar^{TM}), boric acid (H_3BO_3, Merck^{TM}) and poly-vinyl alcohol with a molecular weight of 72,000 (PVA, Merck^{TM}) all in powder form were selected as starting materials. Aqueous solution of 1 M zinc acetate (hereafter $Zn(Ac)_2$) was prepared by dissolving it in distilled water (50 mL). For the preparation of samples having binder, PVA was added into the zinc acetate solution in granular form and stirred at 80 ^oC for 1 hour. Then, $AgNO_3$ or H_3BO_3 was added into the solution to meet target compositions and additional half an hour stirring was applied to obtain homogeneous and stable solutions. All prepared solutions were spray dried prior to thermal decomposition using a laboratory-scale spray dryer (Büchi B-290). During spray drying experiments, 100% aspiration capacity, 15% pumping rate, 4 bar spray flow, in the range of 220 °C inlet and 110 °C outlet atomization temperatures were fixed for all the solutions. Thermal decomposition experiments of spray dried granules were realized in a muffle type furnace with a heating rate of 2 °C/min at 300 °C in air atmosphere. The samples were exposed to 12 h dwell time at the peak temperature and then the samples were furnace cooled. Table 1 summarizes the applied sample compositions and their experimental codes used in this study. Besides, a supplementary flow chart is given in Figure 1 to summary the experimental details.

Table 1. Sample compositions and their experimental codes used in this study.

Solution	After Spray Drying	After Thermal Decomposition
$ZnAc_2$	SD1	TD1
$ZnAc_2$ + $AgNO_3$ (1 wt. % Ag doped)	SD2	TD2
$ZnAc_2$ + $AgNO_3$ (6 wt. % Ag doped)	SD3	TD3
$ZnAc_2$ + H_3BO_3 (1 wt. % B doped)	SD4	TD4
$ZnAc_2$ + H_3BO_3 (6 wt. % B doped)	SD 5	TD5
$ZnAc_2$ + 3 wt. % PVA	SD 6	TD6
$ZnAc_2$ + $AgNO_3$ (1 wt. % Ag doped) + 3 wt. %PVA	SD 7	TD7
$ZnAc_2$ + H_3BO_3 (1 wt. % B doped) + 3 wt. %PVA	SD 8	TD8

2.2 Characterization

Advanced characterization technics were applied for the powders after synthesis. For this purpose, following equipment and procedures were applied. Particle size measurements of the powders were conducted using Microtrac^{TM} Stabino Particle Size Distribution. The specific surface area (SSA) of powders prepared in this study was measured using the Brunauer–Emmett–Teller (BET-SSA) method via Quantachrome^{TM} Autosorb-1 MP device. For this purpose, all samples were outgassed for at least 6 h at 80 °C prior to the adsorption measurements. Morphological investigations were performed using a high-resolution SEM (Quanta^{TM} FEG 250). Phase identification was conducted by means of a Bruker^{TM} D8 Advance XRD with Cu Kα (λ=1.5405Å) radiation operating at 40 kV and 35 mA. Diffraction patterns were collected from the scanning angle 2θ of 20 to 80° with a step size of 2°/min and at a speed of 5° min^{-1}. The optical absorbance of the powders synthesized was determined by a Shimadzu^{TM} UVmini-1240 UV-vis Spectrophotometer in the wavelength range between 200 and 800 nm.

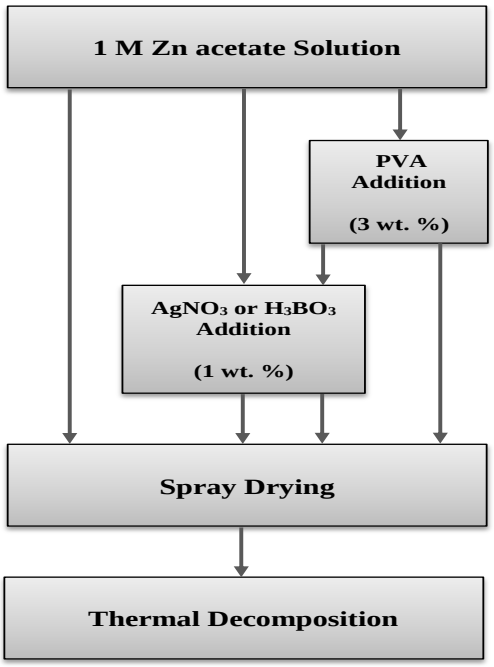

Fig. 1. The flow chart showing the applied procedure for prepared samples.

3. Results and discussion

3.1 Morphological Characterization

SEM micrographs of spray dried sole $Zn(Ac)_2$ solution (SD1) and spray dried $Zn(Ac)_2$ solution having 3 wt. % PVA (SD6) are given comparatively in Figure 2. It is clear that granulation into spherical state was successfully achieved in the presence of PVA. Similar granulation behavior was observed for the doped samples as well.

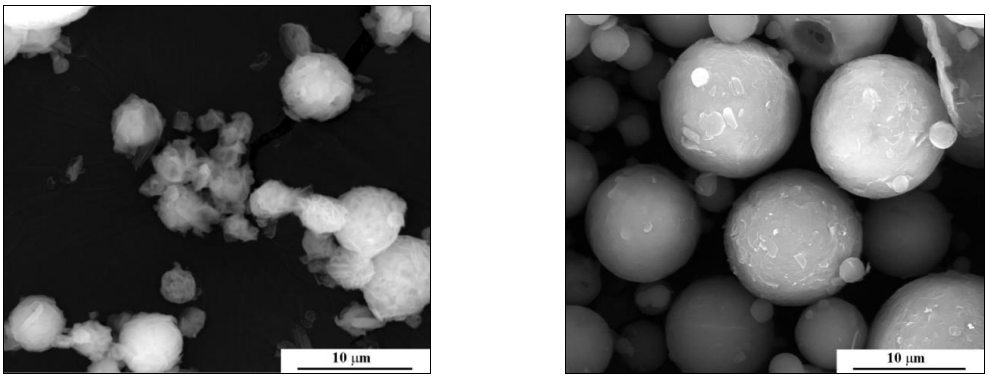

(a) *(b)*

Fig. 2. SEM micrographs of spray dried (a) $Zn(Ac)_2$ *solution (SD1), (b)* $Zn(Ac)_2$ *solution containing 3 wt. % PVA addition (SD6).*

Morphological differences and different sizes of the ultimate powders were observed during characterization by SEM. It is revealed that the powders consisted of the mixture of nanoparticles with the particle sizes of ~150–310 nm and nanorods with diameters of ~50–90 nm and 200–650 nm in length. Micrographs of the spray dried powders after thermal decomposition are given in Figure 3 and Figure 4. In parallel to decomposition reaction of zinc acetate into ZnO, spherical morphology of spray dried granules was destroyed and new particles in nanosize range were formed. It is clear from the micrograph (Fig. 3a) that direct decomposition of zinc acetate in the absence of dopants and PVA does not lead to a characteristic morphology. On the other hand, in the presence of PVA characteristic rod shaped morphology was obtained after thermal decomposition (Fig. 4a). While doping with 1 wt. % $AgNO_3$ (Figure 3b and 4b) led to shorter and thicker rods, doping with 1 wt. % H_3BO_3 (Figure 3c and 4c) led to longer and thinner rods.

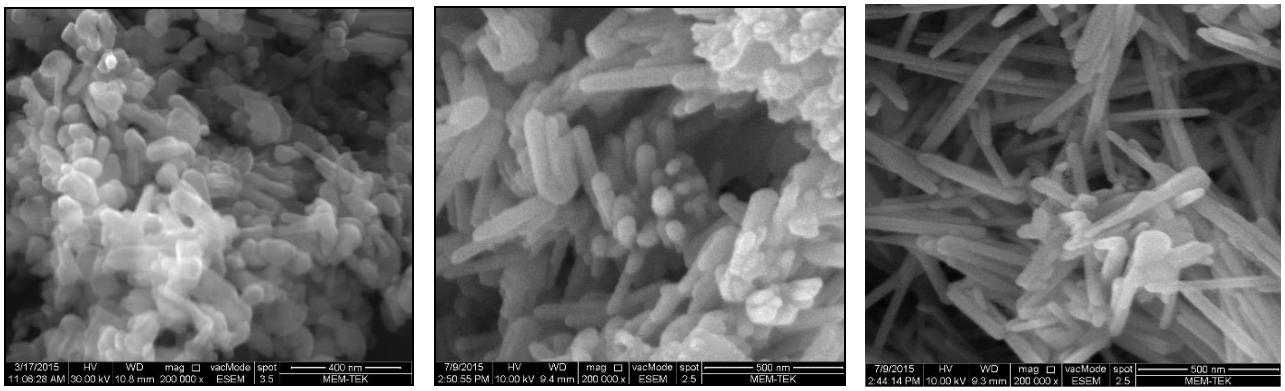

(a) (b) (c)

Fig. 3. SEM micrographs of undoped and doped ZnO-PVA nanoparticles: a) TD1, b) TD2 and c) TD4.

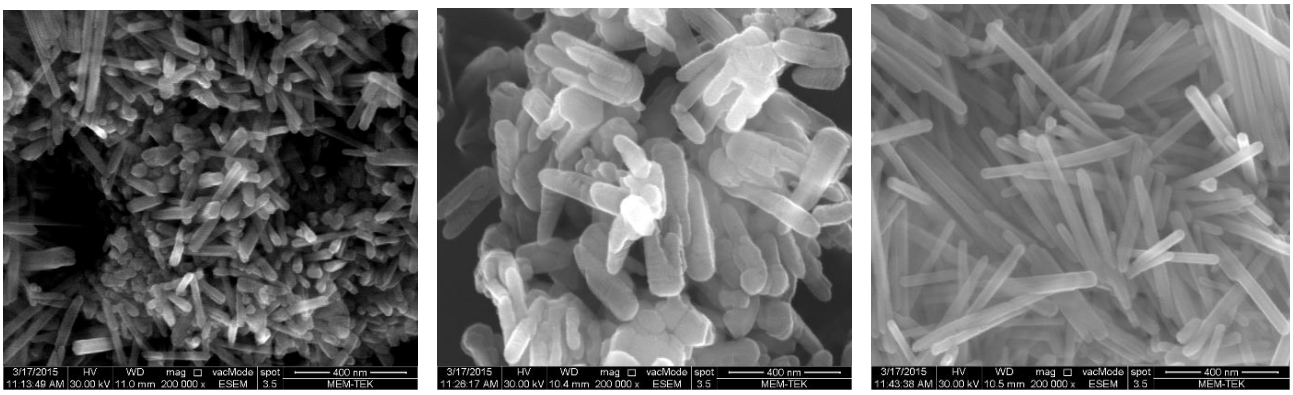

(a) *(b)* *(c)*

Fig. 4. SEM micrographs of undoped and doped ZnO-PVA nanoparticles: a) TD6, b) TD7 and c) TD8.

Since the all powders synthesized do not show characteristic morphology and most of the particles show fiber like morphology different particle size analysis technics were simultaneously applied. For this purpose, laser light scattering and microscopic evaluations were used. For the evaluation of fibers, both length and diameter of the particles were calculated from the analysis of SEM micrographs and further L/D ratios were computed.

It is clear that the average particle size values measured via laser diffraction and the average of L and D values calculated from SEM images show no coherency. It is known that laser light diffraction technics are open to many errors like agglomeration of particles during measurement. On the other hand, microscopic technics are also open to some possible calculation errors like sampling and operational. Therefore, the results in Table 2 are given for a general comparison purpose between the samples rather than representing the exact sizes of the particles obtained.

When the calculated L/D ratios are compared with the corresponding SEM images relatively good agreement is observed. Highest L/D ratios were obtained for the samples TD6 and TD8 showing both PVA and H_3BO_3 are effective for obtaining longer ZnO fibers. While PVA addition led to increase in L/D ratios of the H_3BO_3 doped sample, similar improvement was not observed for $AgNO_3$ doping.

A slight decrease was observed in the surface area values of doped powders having no PVA addition. Addition of PVA led to increase in surface area values for doped powders. However, the similar increasing trend was not observed in the absence of dopants. It is clear from literature both morphology and size of the final ZnO particles and fibers can be altered by changing process conditions [21, 29, 30]. Based on the processing conditions explored in this study, it is also demonstrated that these properties can also be altered by addition of PVA and dopants during spray drying prior to thermal decomposition.

Physical properties of powders after thermal decomposition process are summarized in Table 2.

Table 2. Nanoparticle size and surface area of the synthesized samples by thermal decomposition of the spray dried powders.

Sample Code	Average Particle Size (nm)	Particle Size – length (L) (nm)	Particle Size – diameter (D) (nm)	L/D Ratio	SSA-BET (m^2/g)
Sample 1 (TD1)	306	204.9	82.1	2.5	18.50
Sample 2 (TD2)	297.1	314.4	66.3	4.7	17.05
Sample 4 (TD4)	183.9	393.3	42.1	9.3	15.51
Sample 6 (TD6)	247.2	613.9	50.2	12.2	17.03
Sample 7 (TD7)	214	273.1	87.4	3.1	19.60
Sample 8 (TD8)	241.2	489.0	44.6	11.0	24.18

3.2 Phase analysis

The effect of thermal decomposition on the structure of powders was determined by XRD analysis. XRD results showing the effect of $AgNO_3$ doping both in the presence of PVA and in the absence of PVA are given in Figure 5(a) against undoped sample. XRD results showing the effect of H_3BO_3 doping both in presence of PVA and in the absence of PVA are given in Figure 5(b) against undoped sample. XRD results showing the effect of PVA both undoped and doped samples are given in Figure 5(c). In all samples studied, characteristic ZnO peaks which is good agreement with the JCPDS card no. 70-8070 (wurtzite hexagonal phase) was detected as major phase.

In order to understand the stable phases of the dopants after thermal decomposition, samples were prepared with use of excess amount of dopant. For this purpose, 6 wt. % $AgNO_3$ and 6 wt. % H_3BO_3 additions were realized before spray drying. XRD results after thermal decomposition of these samples are given in Figure 6(a) and 6(b). As it can be seen from these graphs, in addition to peaks belonging to ZnO wurtzite hexagonal phase two small peaks appeared for both cases (at 2θ values of 38.12^o and 44.31^o for 6 wt. % $AgNO_3$ doped sample and at 37.2^o and 42.5^o for 6 wt. % H_3BO_3 doped sample). After peak fitting for possible Ag containing phases, it is concluded that these peaks belonging to (111) and (200) planes of fcc metallic Ag (JCPDS card no. 89-3722).

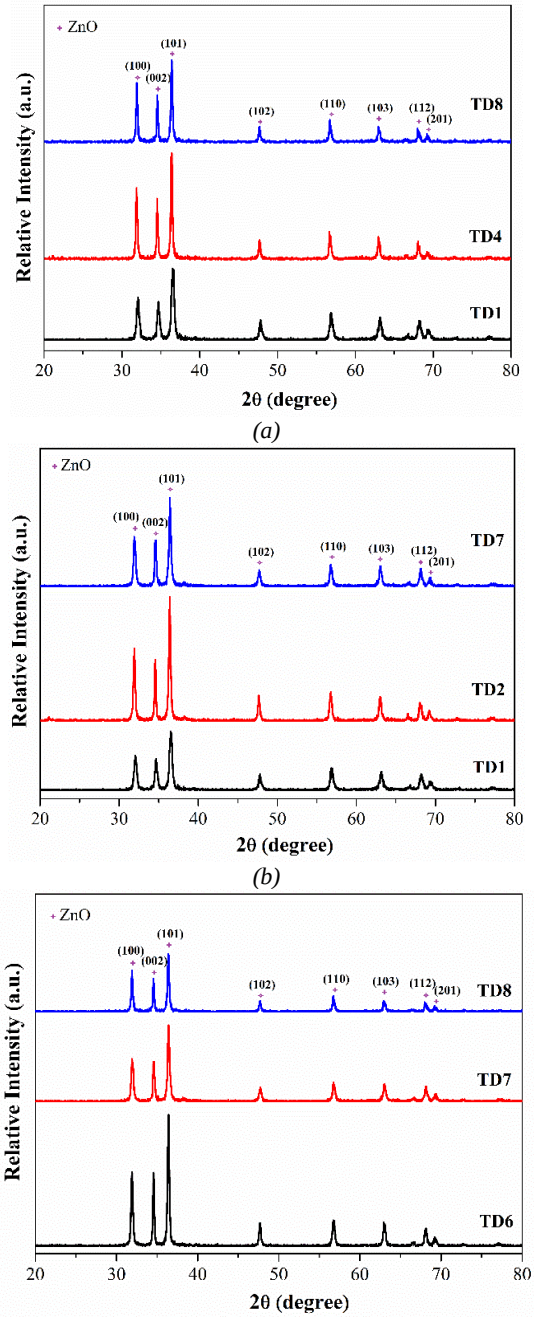

Fig. 5. XRD patterns of the synthesized samples by thermal decomposition of the spray dried powders: (a) $AgNO_3$ doping, (b) H_3BO_3 doping and (c) PVA both undoped and doped samples.

In the case of H_3BO_3 these extra peaks were fitted (014) and (021) planes of B_7O (JCPDS card no. 50-0850). Therefore, it is clear that during heat treatment process, while $AgNO_3$ decomposes into Ag, H_3BO_3 decomposes into B_7O. No additional peak was observed other than ZnO Ag and BO_7 indicating partial decomposition or by-product formation.

In Table 3, the intensity of the peaks of the undoped ZnO decreased with incorporation of silver and boron dopant into the ZnO wurtzite lattice like a substitute atom. It has been notified in literature that foreign particle incorporation like Ag and B in the crystal lattice will induce to production a strain and an expansion of the ZnO lattice [31]. However, the synthesized samples incorporated PVA binder indicates shifting of peak toward lower 2θ value. The shift of peaks to lower angles is led by the strain of the lattice constants which is clearly seen in Table 3.

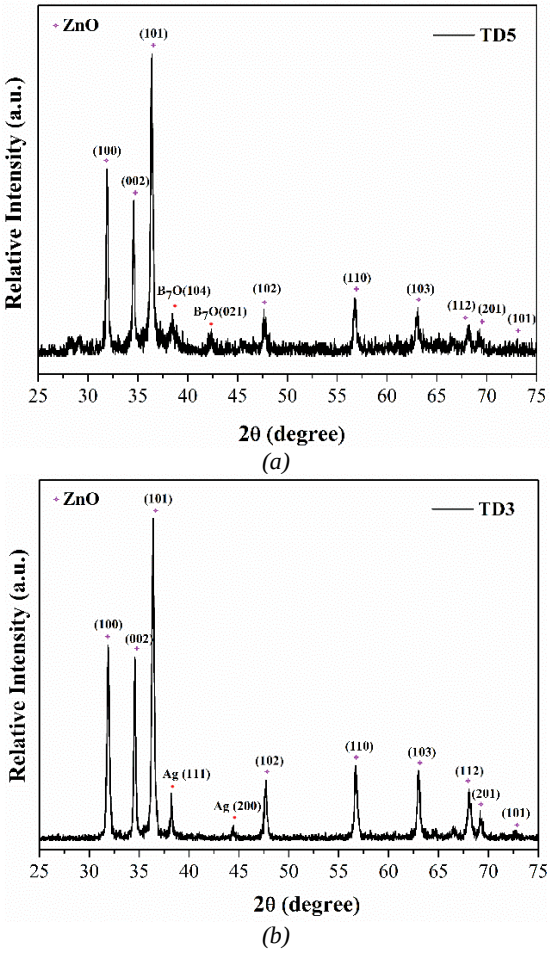

Fig. 6. XRD patterns of the synthesized samples by thermal decomposition of the spray dried powders: (a) TD5 and (b) TD3.

Table 3. XRD parameters of the synthesized samples by thermal decomposition of the spray dried powders.

Sample Code	2θ	hkl	Crystallite Size (nm)
TD1	36.871	(101)	28.1
TD2	36.859	(101)	46.8
TD4	36.448	(101)	40.0
TD6	36.632	(101)	54.5
TD7	36.628	(101)	43.5
TD8	36.421	(101)	45.8

The effect of Ag and BO_7 doping on the mean crystallite size was estimated from the Debye-Scherrer equation [32] as follows:

$$D = \frac{k\lambda}{\beta \cos\theta} \quad (1)$$

where, β = FWHM, θ is Bragg angle, λ = 1.54˚A (X-ray wavelength) and k = 0.9. The crystallite size of the synthesized samples by thermal decomposition of the spray dried powders are estimated and seen in Table 3. As it can be seen from Table 3, the crystallite size increases, as 2θ value decreases.

3.3 UV-Visible absorption study

Effect of dopant and binder on optical properties of the synthesized samples by thermal decomposition of the spray dried powders was determined by UV-vis Spectrophotometric analysis at room temperature. UV-vis peaking values showing the effect of $AgNO_3$ doping both in presence of PVA and in the absence of PVA are given in Fig. 7(a) against undoped sample. UV-vis peaking values showing the effect of H_3BO_3 doping both in presence of PVA and in the absence of PVA are given in Figure 7(b) against undoped sample. UV-vis peaking values showing the effect of PVA both undoped and doped samples are given in Figure 7(c). The spectra reveal a characteristic absorption peak of ZnO, at wavelengths from 360 to 380 nm for the synthesized all samples. As can be seen in Fig.7 (a-b), it is evident that the undoped ZnO nanoparticles showed well-defined absorption band peaking at 375 nm indicating a single and the characteristic band peak for the wurtzite hexagonal structure of ZnO [33]. This value changed in comparison to the absorbance peak value of ZnO [34], probably due to the quantum confinement effect. In Fig.7(c), sample 8 (TD8) has not shown any significant absorbance peak value. The absorption peaks of undoped and doped ZnO and undoped and doped ZnO-PVA nanoparticles having lower intensity was observed, got shifted towards higher energy values.

4. Conclusions

By following spray drying and thermal decomposition processes consecutively it is possible to produce ZnO powders having different morphologies and sizes. It is demonstrated under constant processing conditions that these properties can be altered by addition of PVA and dopants without changing the structure of ZnO. On the other hand, resultant powders having same structure showed certain different optical properties which can be demanded by different engineering needs.

Irregular powder morphology obtained after decomposition of sole zinc acetate transformed to regular fiber morphology in presence of PVA and dopants. It is proved that either PVA or dopant used in this study is individually effective for obtainment of regular fiber morphology. On the other hand, PVA addition is an effective way to improve granulation behaviour during spray drying and fiber formation during thermal decomposition without leaving any residual product. The results show that ZnO nanofibers having different L/D ratios and surface area values can be attained with the proper adjustment of additives.

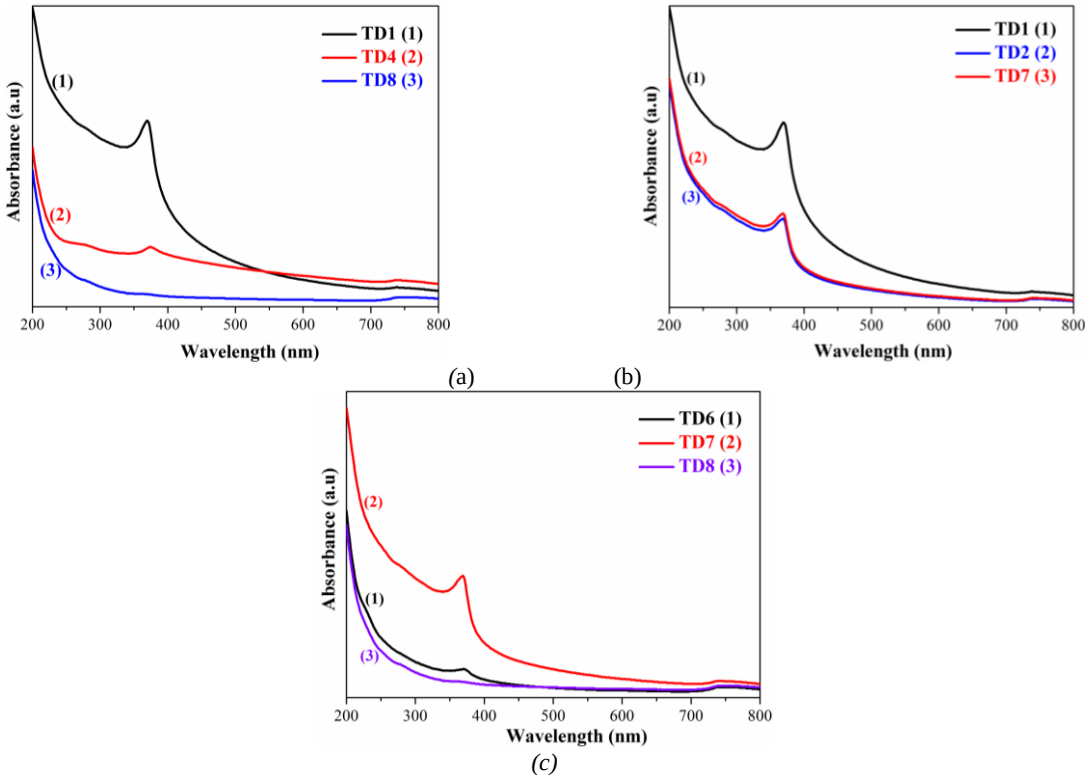

Fig. 7. UV-vis peaking values of the synthesized samples by thermal decomposition of the spray dried powders: (a) $AgNO_3$ doping, (b) H_3BO_3 doping and (c) PVA both undoped and doped samples.

Acknowledgements

This research has been financially supported by the Istanbul Technical University Research Fund (ITU-BAP) under the Project No. 36459 is gratefully acknowledged. Authors would like to thank MSc. Aydın Şelte, MSc. Hadi Jahangiri and MSc. Merve Küçük for their great contribution.

References

[1] S. J. Pearton, D. P. Norton, K. Ip, Y. W. Heo, T. Steiner, Prog. Mater. Sci. **50**, 293 (2005)
[2] M. Sima, I. Enculescu, E. Vasile, J. Optoelectron. Adv. M. **8**, 825 (2006)
[3] S. Khosravi-Gandomani, R. Yousefi, F. Jamali-Sheini, N. M. Huang, Ceram. Int. **40**, 7957 (2014).
[4] F. Jamali-Sheini, R. Yousefi, M. A. More, D. S. Joag, Mater. Lett. **111**, 181 (2013)
[5] C. Gümüş, O. M. Ozkendir, H. Kavak, Y. Ufuktepe, J. Optoelectron. Adv. M. **8**, 299 (2006)
[6] M. Willander, O. Nur, O.X. Zhao, L.L. Yang, M. Lorenz, B.Q. Cao, J.Z. Pérez, C. Czekalla, G. Zimmermann, M. Grundmann, A. Bakin, A. Behrends, M. Al-Suleiman, A. El-Shaer, A. Che Mofor, B. Postels, A. Waag, N. Boukos, A. Travlos, H.S. Kwack, J. Guinard, DLS Dang, Nanotechnology **20**, 332001 (2009)
[7] S. B. Rana, P. Singh, A. K. Sharma, A. W. Carbonari, R. Dogra, J. Optoelectron. Adv. M. **12**, 257 (2010)
[8] R. Yousefi, F. Jamli-Sheini, Ceram. Int. **38**, 5821 (2012)
[9] B. S. Reddy, S. V. Reddy, P. V. Reddy, N. K. Reddy, J. Optoelectron. Adv. M. Rapid Comm. **6**, 953 (2012)
[10] Ü. Alver, S. Kerli, A. Tanriverdi, H. Yaykaşlı, J. Optoelectron. Adv. M. **17**, 439 (2015)
[11] B. S. Reddy, S. V. Reddy, P. V. Reddy, N. K. Reddy, Y. P. Reddy, Adv. Mater. Lett. **5**, 199 (2014)
[12] I. E. Grey, C. Li, C. M. MacRae, J. Solid State Chem. **127**, 240 (1996)
[13] L. Gao, Y. Zhang, J. M. Zhang, K. W. Xu, Appl. Surf. Sci. **257**, 2498 (2011)
[14] R. Singh, S. G. Kulkarni, N. H. Naik, Adv. Mater. Lett. **4**, 82 (2013)
[15] J. J. Wu, S. C. Liu, Adv. Mater. **14**, 215 (2002)
[16] X. Wang, C. J. Summers, Z. L. Wang, Adv. Mater. **16**, 1215 (2004)
[17] X. Zhong, W. Knoll, Chem. Commun., **9**, 1158 (2005)
[18] T. Q. Liu, O. Sakurai, N. Mizutani, M. Kato, J. Mater. Sci. **21**, 3698 (1986)
[19] E. A. Meulenkamp, J. Phys. Chem. B, **102**, 5566 (1998)
[20] A. Kołodziejczak - Radzimska, T. Jesionowski, Materials **7**, 2833 (2014)
[21] S. Music, A. Saric, S. Popovic, Ceram. Int. **36**, 1117 (2010)
[22] A. Kołodziejczak - Radzimska, T. Jesionowski, A. Krysztafkiewicz, Physicochem. Probl. Mi. **44**, 93 (2010)
[23] D. Kim, J. Jung, J. Eur. Ceram. Soc. **27**, 3177 (2007)
[24] G. Bertrand, P. Roy, C. Filiatre, C. Coddet, Chem. Eng. Sci. **60**, 95 (2005)
[25] X. Q. CaO, R. Vassen, S. Schwartz, W. Jungen, F. Tietz, D. Stöever, J. Eur. Ceram. Soc. **20**, 2433 (2000)
[26] I. Taniguchi, N. Fukuda, M. Konarova, Powder Technol. **181**, 228 (2008)
[27] B. Lin, Z. Wen, Z. Gu, S. Huang, J. Power Sources **175**, 564 (2008)
[28] K. Nakahara, R. Nakajima, T. Matsushima, H. Majima, J. Power Sources **117**, 131 (2003)
[29] A. B. D. Nandiyanto, K. Okuyama, Adv. Powder Technol. **22**, 1 (2011)
[30] M. Vaghayenegar, A. Kermanpur, M. H. Abbasi, Sci. Iran. **18**, 1647 (2011)
[31] A. Faheem, K. Shalendra, A. Nishati, M. S. Anwar, Si Nae Heo, Bon Heun Koo, Acta Mater. **60**, 5190 (2012)
[32] C. Suryanarayana, M. G. Norton, Plenum Publishing Corporation, New York (1998)
[33] H. B. Zeng, W. P. Cai, B. Q. Cao, J. L. Hu, Y. Li, P. S. Liu, Appl. Phys. Lett. **88**, 181905 (2006)
[34] H. B. Zeng, W. P. Cai, Y. Li, J. L. Hu, P. S. Liu, J. Phys. Chem. B. **109**, 18260 (2005)

*Corresponding author: dumanseyma@gmail.com